Materials Research. 2019; 22(2): e20180720
DOI: http://dx.doi.org/10.1590/1980-5373-MR-2018-0720

The Modification of $(Nd_{0.5}Ta_{0.5})^{4+}$ Complex-Ions on Structure and Electrical Properties of $Bi_{0.5}Na_{0.5}TiO_3$-$BaTiO_3$ Ceramics

Runpu Dou[a], Ling Yang[a]*, Jiwen Xu[a,b], Xiaowen Zhang[a], Hang Xie[a],

Changlai Yuan[a,b], Changrong Zhou[a,b], Guohua Chen[a,b], Hua Wang[a,b]

[a]School of Materials Science and Engineering, Guilin University of Electronic Technology, Guilin 541004, China
[b]Guangxi Key Laboratory of Information Materials, Guilin University of Electronic Technology, Guilin 541004, China

Received: November 09, 2018; Revised: January 03, 2019; Accepted: January 23, 2019

The $(Bi_{0.5}Na_{0.5})_{0.94}Ba_{0.06}Ti_{1-x}$ $(Nd_{0.5}Ta_{0.5})_xO_3$ ($0.01 \leq x \leq 0.05$) lead-free ceramics (BNBT-*x*NT) used $(Nd_{0.5}Ta_{0.5})^{4+}$ complex-ions to modify its structure and electrical properties. The BNBT-*x*NT ceramics exhibit the coexistence of tetragonal and rhombohedral phase. The $(Nd_{0.5}Ta_{0.5})^{4+}$ complex-ions prohibit grain growth, and its average grain size decreases from 2.53 μm to 0.84 μm with increasing complex-ion content. The NT doping not only induces the transformation from ferroelectric phase to relaxor ferroelectric phase but also decreases the coercive field and remnant polarization. The permittivity curves are broadened at heavily doping content. The energy storage and strain properties are improved by complex-ions. The maximum energy storage density of 0.475 J/cm^3 is obtained at x = 0.035 and 60 kV/cm, the energy storage efficiency achieves the maximum efficiency of 61.5% at x=0.05. As increasing complex-ion content, the typical butterfly-shaped strain curve develops into a sprout-shaped one, and the maximum strain of 0.199% is obtained at x=0.02.

Keywords: *BNT-BT, $(Nd_{0.5}Ta_{0.5})^{4+}$, Relaxor ferroelectric, Energy storage, Strain.*

1. Introduction

The growing level of environmental awareness makes the researchers try their best to find out lead-free material to take place of the poisonous lead-based ferroelectric ceramics with excellent electrical properties. $Bi_{0.5}Na_{0.5}TiO_3$ (BNT) ceramics have ABO_3 perovskite structure which is deemed to be one of the most potential lead-free candidates for lead-based ceramics due to its outstanding ferroelectric and piezoelectric properties at room temperature [1].

The structure of pure BNT ceramics can be modified, and its properties can also be improved by doping or solid solution. As is reported [2,3], the morphotropic phase boundary (MPB) structure was found out in $Bi_{0.5}Na_{0.5}TiO_3$-$Bi_{0.5}K_{0.5}TiO_3$ (BNT-BKT) and $Bi_{0.5}Na_{0.5}TiO_3$-$BaTiO_3$ (BNT-BT) systems, which can obtain better electrical properties [4-8]. The Nd_2O_3 doped $0.82Bi_{0.5}Na_{0.5}TiO_3$-$0.18Bi_{0.5}K_{0.5}TiO_3$ ceramics obtained the excellent piezoelectric properties (d_{33}=134pC/N, K_p=0.27)[9]. The value of piezoelectric constant increased to 170pC/N from 150pC/N by doping $Ta^{(5+)}$ into $0.94Bi_{0.5}Na_{0.5}TiO_3$-$0.06BaTiO_3$ ceramics according to Han's study [10]. What's more, the complex-ions doped BNT-based ceramics also illustrated interesting microstructure, phase structure transition and excellent electrical properties. The average grain size of BNBT-*x*PN ceramics decrease from 1.55 μm to 0.95 μm after doping the $(Pr_{0.5}Nb_{0.5})^{4+}$ complex-ions [11]. The $(Al_{0.5}Nb_{0.5})^{4+}$ modified BNT-BKT ceramics shown a high energy storage density of 1.41 J/cm^3 [12]. The BNT-BT ceramics doped by $(Fe_{0.5}Nb_{0.5})^{4+}$ shown a highest unipolar strain of 0.422% [13]. For the BNBT6.5-*x*AS ceramics, a phase transition occurred from ferroelectric to relaxor phase with increasing $(Al_{0.5}Sb_{0.5})^{4+}$ contents [14]. Therefore, the local hetero structure constructed by complex-ions can induce its electrical properties improvement or transition.

The $Ca_{0.61}Nd_{0.26}Ti_{1-x}$ $(Cr_{0.5}Ta_{0.5})_xO_3$ microwave ceramics were modified by $(Cr_{0.5}Ta_{0.5})^{4+}$ complex-ions, which show the good and stable comprehensive microwave dielectric properties [15]. The ionic radius of Ta^{5+} (0.640 Å) is close to that of Ti^{4+} (0.605 Å). However, the Nd^{3+} with larger ionic radius (0.983 Å) was used to induce lattice distortion. So the $(Nd_{0.5}Ta_{0.5})^{4+}$ complex ions were designed to modify the structure of BNT-based ceramic and improve its electrical properties.

*e-mail: lingyang@guet.edu.cn

In this work, the $(Bi_{0.5}Na_{0.5})_{0.94}Ba_{0.06}Ti_{1-x}(Nd_{0.5}Ta_{0.5})_xO_3$ ceramics (BNBT-*x*NT) were modified by $(Nd_{0.5}Ta_{0.5})^{4+}$ complex-ions, and its microstructure, crystal structure, ferroelectric, energy storage properties, dielectric, field-induced strain response and impedance were studied.

2. Experiments

The BNBT-*x*NT (*x*=0.01, 0.02, 0.03, 0.035, 0.04, 0.05) ceramics were prepared by using Bi_2O_3 (99.95%), Na_2CO_3 (99.8%), $BaCO_3$ (99%), TiO_2 (99.9%), Nd_2O_3 (99.95%) and Ta_2O_5 (99.99%) dried powders as the starting raw materials. All oxide powders were weighed according to the stoichiometric formula. And according to our previous work [16], after ball milling in ethanol with ZrO_2 balls for 12 hours, the powders were dried at 90 °C for 24 hours and then calcined at 880 °C for 2 hours. The powders added polyvinyl alcohol aqueous solution (7 wt%) as binder were granulated by 100-mesh sieve. The green bodies with a diameter of 13 mm and a thickness of 1.0 mm were pressed under 40 MPa. The sintered bodies were sintered in air at 1150 °C for 2 hours. The electrical test samples were polished to 0.5mm in thickness and fabricated Ag electrodes on both sides at 580 °C for 30 minutes.

The crystal structure of BNBT-*x*NT samples was characterized by X-ray diffractometer (XRD, D8-Advance, Bruker). The surface morphology and grain size were analyzed by Filed-Emission Scanning Electron Microscope (FESEM, qunata 450 FEG, FEI). The electric-field-induced polarization (*P*-*E*), bipolar strain (*S*-*E*) and current-electric field (*I*-*E*) were measured by ferroelectric test system (TF Analyzer-2000E, aixACCT). The energy storage properties were calculated by integrating the *P*-*E* loop. The dielectric constant and loss were measured by impedance analyzer (4294A, Agilent) with a heating rate of 2 °C/min from room temperature to 400 °C, and the impedance spectrum was also measured by impedance analyzer.

3. Results and Discussion

Figure 1 is the XRD patterns of BNBT-*x*NT ceramics with *x*=0.01-0.05. The XRD patterns reveal all of the diffraction peaks are indexed by $(Na_{0.5}Bi_{0.5})TiO_3$ (JCPDS No.46-0001), which indicates the formation of perovskite single phase structure without other impurity phases. Therefore, the Nd^{3+} and Ta^{5+} ions diffused into the lattice of matrix and formed solid solution. As previous report [17], the pure $Bi_{0.5}Na_{0.5}TiO_3$ and $BaTiO_3$ are rhombohedral and tetragonal structure, respectively. As shown in Figure 1 (b), the (111) peak at about 40° splits into the (003) and (021) peaks which proves the existence of rhombohedral phase structure. The (200)/(002) splitting peaks at 46°-47° as shown in Figure 1 (c) indicates tetragonal phase structure [18]. The peaks shift to lower diffraction angles with the increasing amounts of NT complex-ions. The reason of peak shifting is that the ionic radius of Ti^{4+} (0.0605 nm) at B-site are smaller than Nd^{3+} (0.0983 nm) and Ta^{5+} (0.0640 nm) [19,20]. Thus the lattice distortion induces the change of lattice constant, and the diffraction peak shifts to lower angle according to the Bragg law. According to the two splitting peak behaviors, it can be concluded that the rhombohedral and tetragonal phase structure coexist in the BNBT-*x*NT ceramics [21,22].

The surface morphologies and grain size distribution of BNBT-*x*NT ceramics with *x*=0.01-0.05 is shown in Figure 2. The grain size of BNBT-*x*NT ceramics was measured by the calculation software "nano measurer". The grains and grain boundaries observed from SEM images are clear. The shape of grains from top view shows circular-like structure. However, the ceramic samples show a small number of pores. These pores can affect breakdown electric field because these defects are preferentially broken down. When *x*=0.01, the grain size illustrates a wide range from 1.0 μm to 6.0 μm. As the complex-ion content increase, the range of grain size gradually becomes smaller, and the same phenomenon can be observed in Nb/In co-doped $Bi_{0.49}La_{0.01}Na_{0.49}Li_{0.01}TiO_{3-\delta}$ ceramics [23]. And the average grain size of BNBT-*x*NT ceramics decrease slightly from 2.53 μm at *x*=0.01 to 0.84 μm at *x*=0.05, which implies the $(Nd_{0.5}Ta_{0.5})^{4+}$ complex-ions are grain growth inhibitor for BNBT ceramics. The grain growth of 0.94BNT-0.06BT ceramics was not evidently affected by Ta-doping [24]. However, the grain size of Nd doped BNT ceramics shown an obvious decrease [20]. And the grain size of Nd doped 0.82BNT-0.18BKT ceramics decreases slightly [9]. The reason is that the segregation of some Nd^{3+} ions at grain boundaries, which prevents grain boundary movement during sintering and inhibits grain growth [9]. Therefore, the grain growth behavior of BNBT-*x*NT ceramics in this work can attribute to the same reasons.

Owning to the breakdown electric field of BNBT-0.01NT ceramic is under 70 kV/cm, so the *P*-*E* hysteresis loops of the BNBT-*x*NT ceramics were tested at 60 kV/cm and 1 Hz as shown in Figure 3(a). And the Figure 3(b) is the evolution of the coercive field (E_c), remnant polarization (P_r), maximum polarization (P_{max}) and ΔP (P_{max}-P_r) for BNBT-*x*NT ceramics. It can be seen that the P_{max} and P_r simultaneously decrease with increasing NT complex-ion content, and the change of the E_c is not obvious. When *x*=0.01, the E_c, P_r and P_{max} observed from the *P*-*E* loop are 29.4 kV/cm, 26.9 μC/cm^2 and 34.4 μC/cm^2, respectively. And then the P_r and E_c suddenly decrease to 8.4 μC/cm^2 and 14.7 kV/cm at *x*=0.02. After that the P_r, P_{max} and E_c gradually decrease along with the increase of complex-ion content. Lastly, the BNBT-*x*NT ceramics obtain the minimum P_r of 1.97 μC/cm^2 and E_c of 10.61 kV/cm at *x*=0.05. The ferroelectric behavior transformation lies in that the NT complex-ions disturb the long-range ferroelectric order and the relaxor characteristics increased [11].

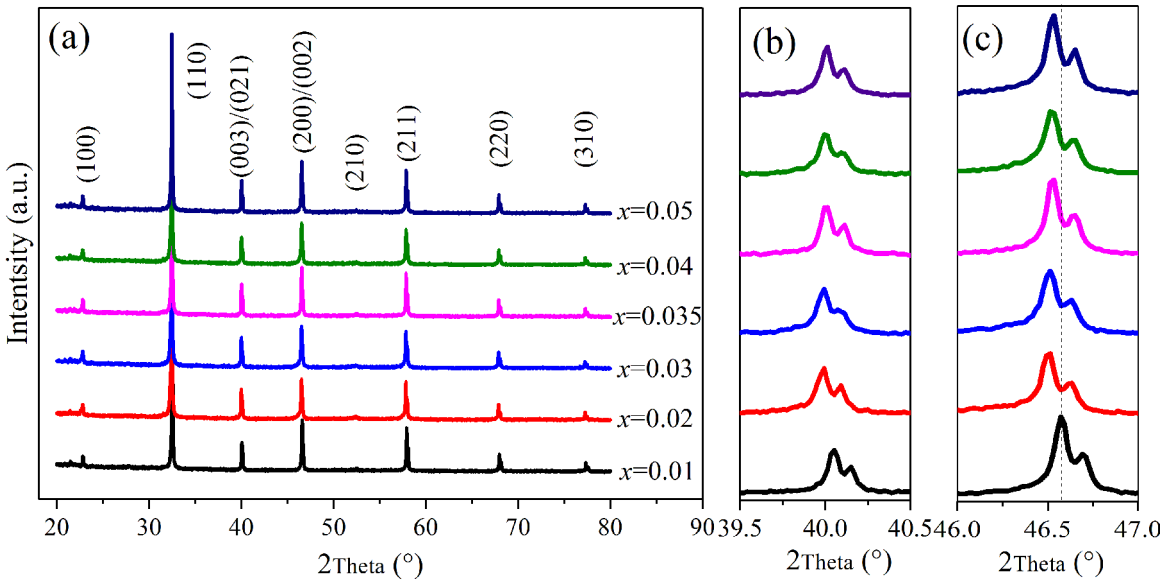

Figure 1. XRD patterns of BNBT-*x*NT ceramics at (a) 20°-80°, (b) 39.5°-40.5° and (c) 46°- 47°

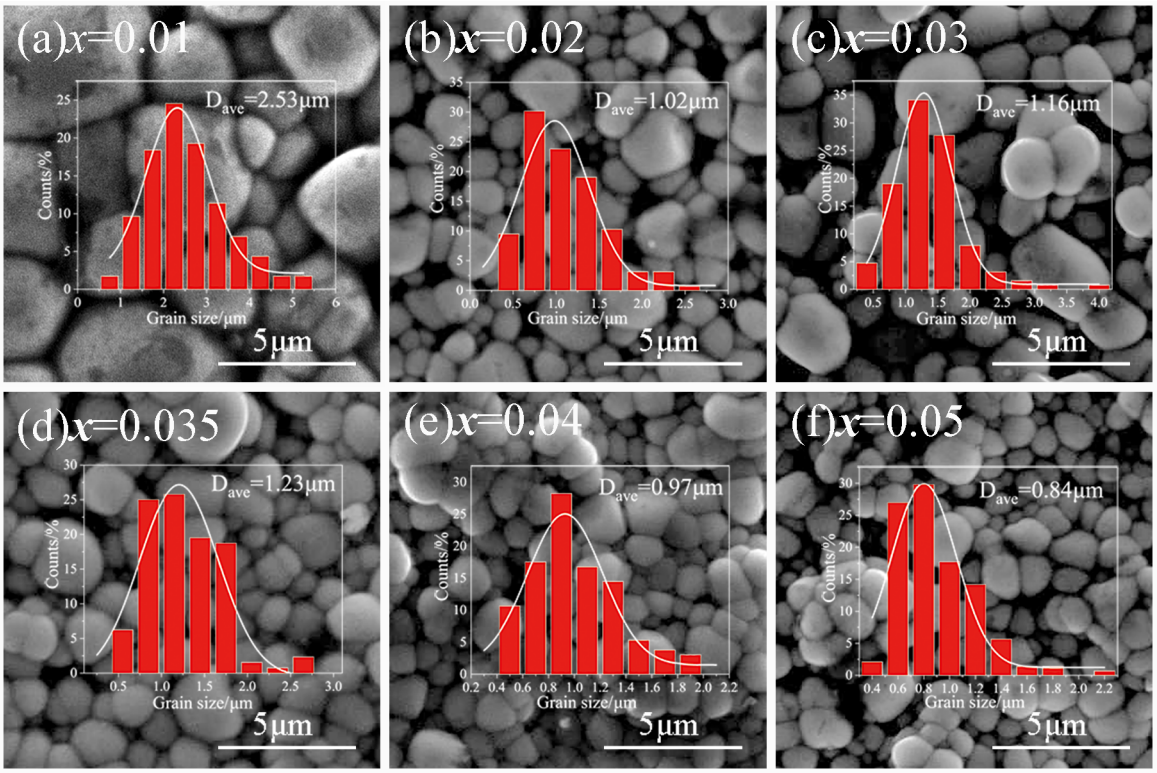

Figure 2. Surface morphologies and grain size distribution of BNBT-*x*NT ceramics

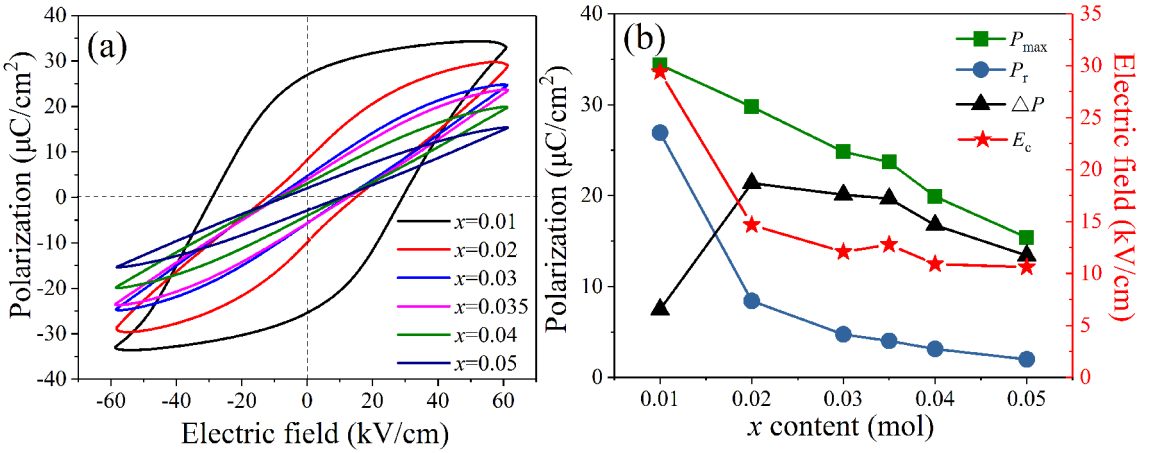

Figure 3. (a) Hysteresis loops of BNBT-*x*NT ceramics tested at 60 kV/cm and (b) ferroelectric properties (P_{max}, P_r, ΔP, E_c)

The following formula can be used to calculate the energy storage density (W) and energy storage efficiency (η)[25]:

$$W = \int_{P_r}^{P_{max}} EdP \quad (1)$$

$$\eta = \frac{W_1}{W_1 + W_2} \times 100\% \quad (2)$$

Where W_1 is the electrical energy storage density, E refers to the applied external electric filed, P_r and P_{max} are the remnant and maximum polarization. W_2 is the energy absorption density and η is energy storage efficiency.

Figure 4 exhibits the energy storage density and efficiency of BNBT-*x*NT ceramics which are calculated from the *P-E* loops at 60 kV/cm and 1 Hz. The improvement of energy storage properties is attributed to the transition of ferroelectric behavior. For x=0.01, the energy storage density is 0.126J/cm^3 and efficiency is 8.3% (P_{max}=34.4 μC/cm^2, P_r=26.9 μC/cm^2, ΔP=7.5 μC/cm^2, E_c=29.4 kV/cm). Then as shown in Figure 3, the *P-E* loop becomes slim and the ΔP sharply increases when x=0.02, so the ferroelectric properties decrease. Thus, according to the formula (1) and (2), the energy storage density and efficiency have an obvious improvement to 0.418J/cm^3 and 35.6%. At x=0.035, the energy storage density goes up to the maximum value of 0.475 J/cm^3 (P_{max}=23.69 μC/cm^2, P_r=4.01 μC/cm^2, ΔP=19.67 μC/cm^2, E_c=12.78 kV/cm). With the further increase of complex-ion content, the energy storage density gradually decreases. At the same time, the energy storage efficiency is always increasing and achieves the maximum efficiency of 61.5% at x=0.05.

Figure 5 shows the current-polarization-electric field (*I-P-E*) of BNBT-*x*NT ceramics tested at 60 kV/cm and 1 Hz. When x=0.01, there are only two current peaks which correspond to $+E_c$ and $-E_c$ for the *P-E* curve. The reason for appearance of two current peaks is the domain switching of typical ferroelectric at the E_c value of the external electric

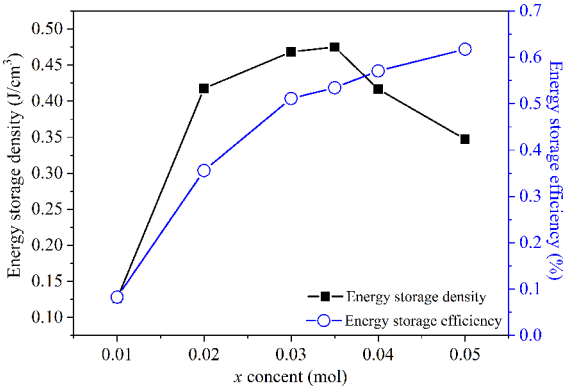

Figure 4. Energy storage density and efficiency of BNBT-*x*NT ceramics

field [26]. Thus, the current peaks, large P_r and E_c indicate that the ferroelectric phase is dominant for BNBT-*x*NT at x=0.01 [27]. However, four peaks I_1 and I_2 be appeare for each *I-E* loops when x>0.01 and indicates the phase transition of BNBT-*x*NT ceramics. The current peak of I_1 represents the relaxor-ferroelectric transition, while the current peak of I_2 corresponds to the ferroelectric-relaxor transition [28]. Therefore, BNBT-*x*NT ceramics are dominated by relaxor ferroelectric phase when x>0.01. With the increase of complex-ion content, all the four current peaks become weak, and the P_{max} declines. The reason is that the high concentration complex-ions lead to the rising proportions of relaxor ferroelectric phase than that of the ferroelectric phase [29].

Figure 6 reveals the bipolar field-induced strains of BNBT-*x*NT ceramics tested at 60 kV/cm. It can be seen that the positive strain shows a little increase from 0.191% to 0.199% when the NT content increased to 0.02. Further increasing NT content, the positive strain shows an obvious decrease from 0.177% to 0.061%. Meanwhile, the negative strain (S_{neg}=0.186%) only appears at x=0.01 and exhibits butterfly characterization, which is mainly related to the dominant ferroelectric phase for the structure [30]. But the

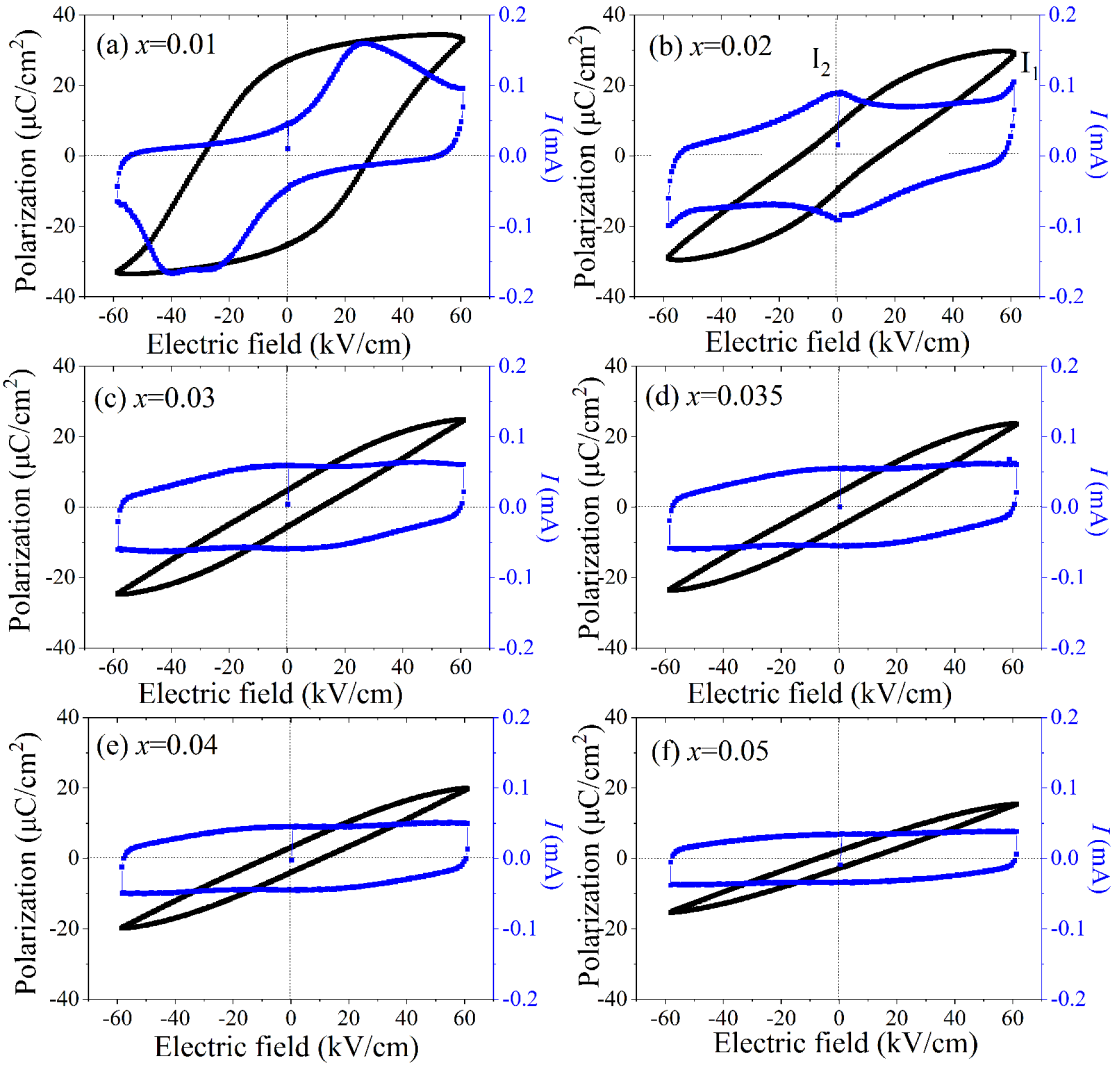

Figure 5. *P-E* and *I-E* loops of BNBT-*x*NT ceramics

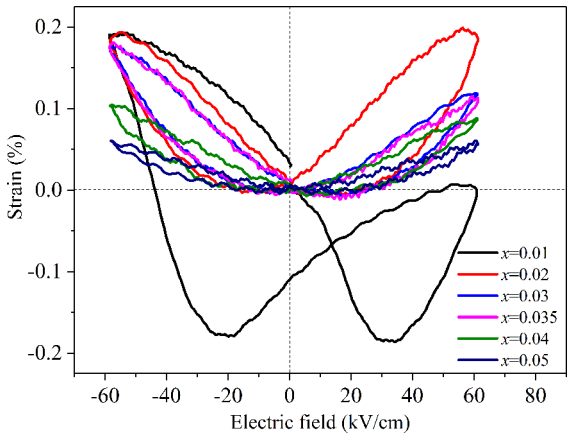

Figure 6. *S-E* loops of BNBT-*x*NT ceramics

butterfly-shaped curve is apparently asymmetric under the effect of internal bias electric field resulting from the formation of defect dipoles during sintering, while the defect dipoles come from the NT doping [31]. The internal bias field and external electric field interact together during bipolar strain test. The actual electric field in samples is the result of their interaction. The internal bias field plays different role to strengthen or weaken external electric field according to their direction. As the doping content increase, it can be seen that the typical butterfly-shaped strain curve develops into a sprout-shaped one and the S_{neg} disappears, which indicates the BNBT-*x*NT ceramics with ferroelectric phase transform to the relaxor ferroelectric phase [32].

The temperature dependence of relative permittivity (ε_r) and loss (tanδ) of BNBT-xNT ceramics at frequencies of 1 kHz, 10 kHz and 100 kHz are exhibited in Figure 7. As it is shown, there are two dielectric anomaly peaks (T_p and T_m) for each permittivity curve owing to the thermal evolution of the symmetric ferroelectric polar nanoregions (PNRs) of *R3c* and *P4bm* structure [33]. The T_p dielectric anomaly peak shows a strong frequency dispersion behavior, while the T_m dielectric anomaly peak illustrates weak frequency dispersion [22]. And at the same temperature, the dielectric constant decreases as the frequency increasing. On the other hand, with increasing complex-ion content, the frequency dependence of dielectric permittivity is weakened. The dielectric peaks of T_m indicate the phase transition temperature of BNBT-xNT ceramics from "anti-ferroelectric-like" to paraelectric phase [34]. For the heavily doped BNBT-xNT ceramics, the dielectric peaks of T_m become broader and slightly shift to the lower temperature. These broad dielectric behavior and dependent frequency are characteristic of relaxor ferroelectric [35]. In addition, the value of dielectric loss (tanδ) increases with the rising of frequency at the same temperature. Meanwhile, at the same frequency, the dielectric loss gradually decreases at the temperature range of T_p to T_m. It is probably related to the tiny distortion in crystalline structure after depolarization [36].

To describe the dielectric dispersion and diffuseness of phase transition, the following modified Curie-Weiss law was used in many researches [37,38].

$$\ln(1/\varepsilon - 1/\varepsilon_m) + \ln C = \gamma \ln(T - T_m) \quad (3)$$

The letter C is the Curie constant, ε_m and ε are the maximum dielectric constant and the dielectric constant, and γ is the degree of diffuseness. The range of γ value is from 1 to 2, which corresponds to a normal ferroelectric to an ideal relaxor ferroelectric [39]. Figure 8 reveals the plot of ln(1/ε-1/ε_m) *versus* ln(T-T_m), which can obtain the γ value by data fitting. The γ values of BNBT-xNT ceramics at x>0.01 are extremely close to 2. Its value is between 1.87

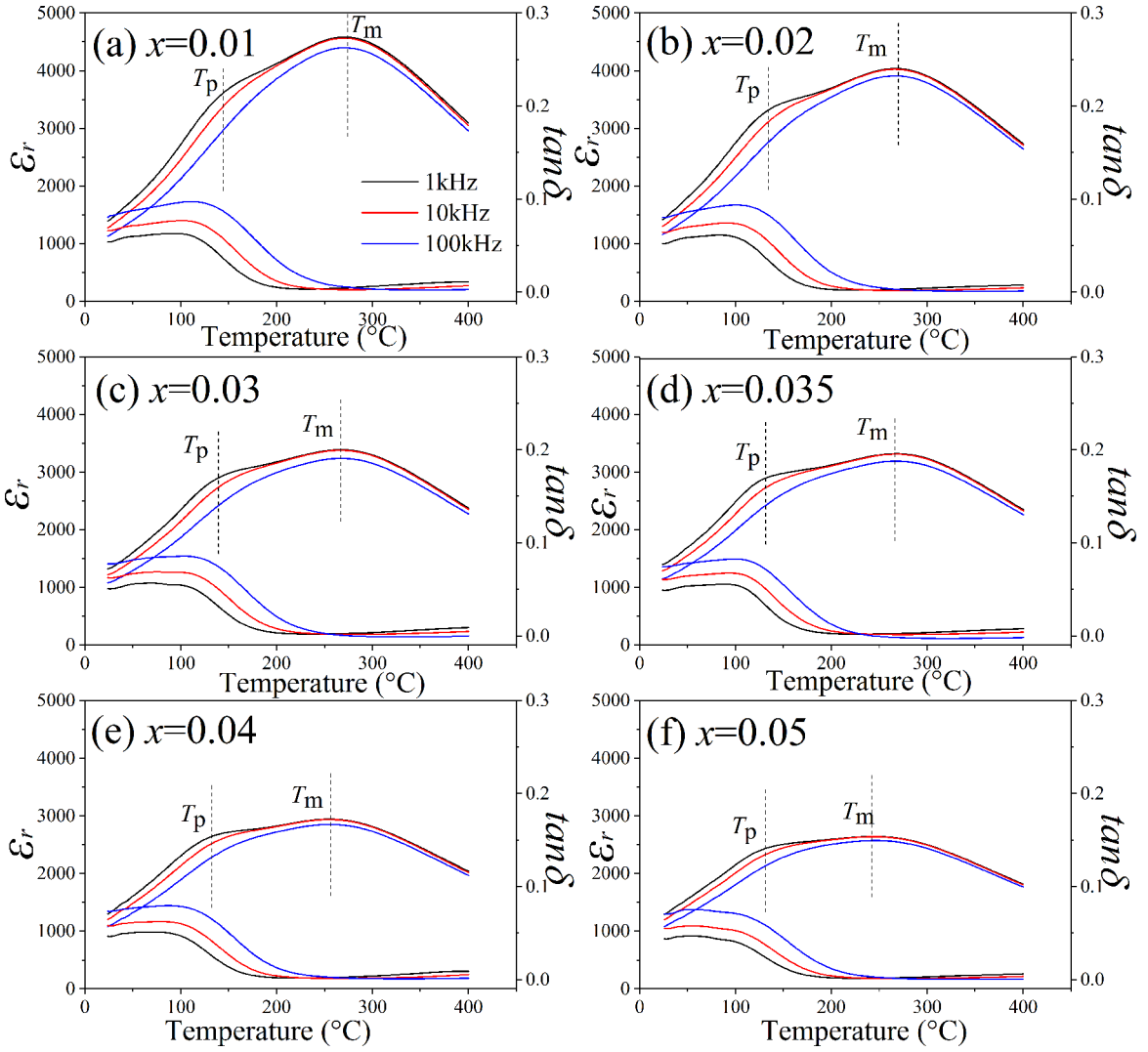

Figure 7. Dielectric constant and loss of BNBT-xNT ceramics as a function of temperature at 1 kHz, 10 kHz and 100 kHz

and 2.08, confirming that the phase transition has a diffuse characteristic, consistent with the *P-E* results shown in Figure 5. The similar relaxor behavior was observed in $0.8(Bi_{0.5}Na_{0.5})TiO_3$-$0.2(Bi_{0.5}K_{0.5})(Hf_x\ Ti_{1-x})O_3$ ceramics with γ value between 1.89 and 2 [40].

Figure 9 shows the Cole-Cole plots of impedance with different temperature from 200 °C to 540 °C for x=0.035. Firstly, the impedance curves are nearly parallel to the ordinate at lower temperature. And then the curves bend towards abscissa and form semicircles as the increasing temperature. The BNBT-0.035NT ceramic presents an excellent insulating capacity below the temperature of 300 °C. Afterwards, the radii of the semicircles become smaller and smaller. The radii of semicircles in Cole-Cole plot represent the resistive behavior of ceramic [16,41]. So it indicates that the conductivity increases and the impedance decreases with heating [11,42]. The increase of conductivity of BNBT-0.035NT ceramic is attributed to the thermal activated carriers.

4. Conclusions

The $(Nd_{0.5}Ta_{0.5})^{4+}$ complex-ions were used to modify the structure and electrical properties of the $(Bi_{0.5}Na_{0.5})_{0.94}Ba_{0.06}Ti_{1-x}(Nd_{0.5}Ta_{0.5})_xO_3$ lead-free ceramics. The BNBT-xNT ceramics are single-phase perovskite structure without impurity phases, and show the coexistence of tetragonal and rhombohedral phase. The average grain size decreases from 2.53 μm to 0.84 μm with increasing complex-ion content. The NT complex-ions decrease the remnant polarization and coercive field. Meanwhile, the relaxor ferroelectric phase of heavily doped BNT-BT ceramics were verified by the evolution of current peak, the disappearing negative strain and diffuseness coefficient. The doping of complex-ions decreases the dielectric constant and broadens the permittivity curves. The maximum energy storage density of 0.475 J/cm^3 is obtained at x=0.035 and 60 kV/cm, and the optimal value of strain is 0.199% obtained at x=0.02. These results reveal that the structure and electrical properties of BNT-BT ceramics can be modified by complex-ions introducing.

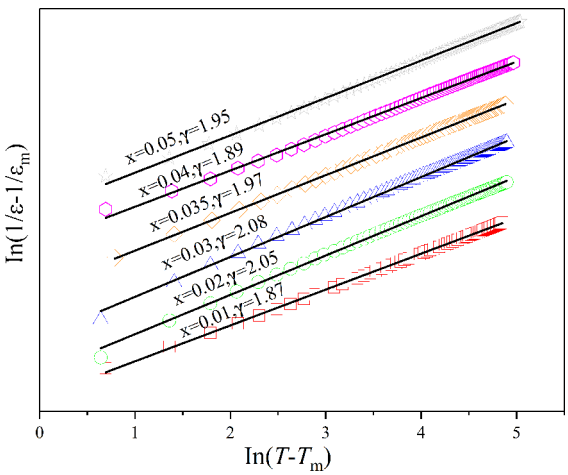

Figure 8. Plot of ln(1/ε-1/ε m) versus ln(T-T_m) of BNBT-xNT ceramics

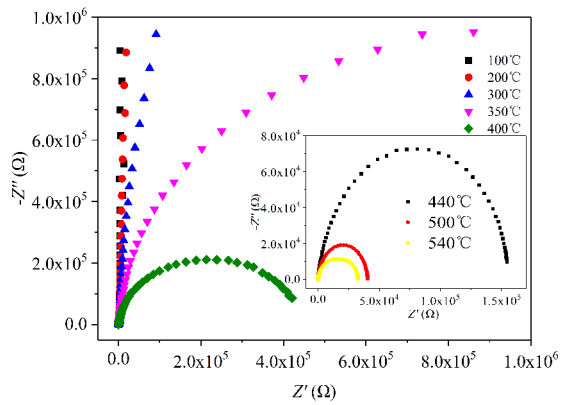

Figure 9. Cole-Cole plots of BNBT-0.035NT ceramic measured from 100 °C to 540 °C

5. Acknowledgements

This work is supported by the National Nature Science Foundation of China (61741105, 11664006), Guangxi Nature Science Foundation (2016GXNSFAA380069) and Guangxi Key Laboratory of Information Materials (161001-Z, 171009-Z).

6. References

1. Li P, Liu B, Shen B, Zhai J, Li L, Zeng H. Large strain response in $Bi_4Ti_3O_{12}$ modified BNT-BT piezoelectric ceramics. *Ceramics International*. 2017;43(1):1008-1013.

2. Jo W, Daniels JE, Jones JL, Tan X, Thomas PA, Damjanovic D, et al. Evolving morphotropic phase boundary in lead-free $(Bi_{1/2}Na_{1/2})TiO_3$-$BaTiO_3$ piezoceramics. *Journal of Applied Physics*. 2011;109(1):014110.

3. Yang Z, Liu B, Wei L, Hou Y. Structure and electrical properties of (1-x)$Bi_{0.5}Na_{0.5}TiO_{3-x}Bi_{0.5}K_{0.5}TiO_3$ ceramics near morphotropic phase boundary. *Materials Research Bulletin*. 2008;43(1):81-89.

4. Zhang H, Xu P, Patterson E, Zang J, Jiang S, Rödel J. Preparation and enhanced electrical properties of grain-oriented $(Bi_{1/2}Na_{1/2})TiO_3$-based lead-free incipient piezoceramics. *Journal of the European Ceramic Society*. 2015;35(9):2501-2512.

5. Chaouchi A, Kennour S, d'Astorg S, Rguiti M, Courtois C, Marinel S, et al. Characterization of sol-gel synthesised lead-free (1-x) $Na_{0.5}Bi_{0.5}TiO_{3-x}BaTiO_3$-based ceramics. *Journal of Alloys and Compounds*. 2011;509(37):9138-9143.

6. Chandrasekhar M, Kumar P. Synthesis and characterizations of BNT-BT and BNT-BT-KNN ceramics for actuator and energy storage applications. *Ceramics International*. 2015;41(4):5574-5580.

7. Pham KN, Hussain A, Ahn CW, Ill KW, Jeong SJ, Lee JS. Giant strain in Nb-doped $Bi_{0.5}(Na_{0.82}K_{0.18})_{0.5}TiO_3$ lead-free electromechanical ceramics. *Materials Letters*. 2010;64(20):2219-2222.

8. Fu P, Xu Z, Zhang H, Chu R, Li W, Zhao M. Structure and electrical properties of Er_2O_3 doped $_{0.82}Bi_{0.5}Na_{0.5}TiO_3$-$0.18Bi_{0.5}K_{0.5}TiO_3$ lead-free piezoelectric ceramics. *Materials & Design*. 2012;40:373-377.

9. Yang Z, Hou Y, Liu B, Wei L. Structure and electrical properties of Nd_2O_3-doped $0.82Bi_{0.5}Na_{0.5}TiO_3$-$0.18Bi_{0.5}K_{0.5}TiO_3$ ceramics. *Ceramics International*. 2009;35(4):1423-1427.

10. Han WH, Koh JH. Shrinkage mechanism and enhanced piezoelectric properties of Ta doped $0.94Bi_{0.5}Na_{0.5}TiO_3$-$0.06BaTiO_3$ lead free ceramics. *Ceramics International*. 2018;44(5):5352-5358.

11. Wang C, Xu Z, Cheng R, Chu R, Hao J, Li W, et al. Electric field-induced giant strain and piezoelectricity enhancement effect in $(Bi_{1/2}Na_{1/2})_{0.935+x}Ba_{0.065}Ti_{1-x}(Pr_{1/2}Nb_{1/2})_xO_3$ lead-free ceramics. *Ceramics International*. 2016;42(3):4354-4360.

12. Zhao Y, Xu J, Yang L, Zhou C, Lu X, Yuan C, et al. High energy storage property and breakdown strength of $Bi_{0.5}(Na_{0.82}K_{0.18})_{0.5}TiO_3$ ceramics modified by $(Al_{0.5}Nb_{0.5})^{4+}$ complex-ion. *Journal of Alloys and Compounds*. 2016;666:209-216.

13. Cheng R, Xu Z, Chu R, Hao J, Du J, Li G. Electric field-induced ultrahigh strain and large piezoelectric effect in $Bi_{1/2}Na_{1/2}TiO_3$-based lead-free piezoceramics. *Journal of the European Ceramic Society*. 2016;36(3):489-496.

14. Li L, Hao J, Xu Z, Li W, Chu R. 0.46% unipolar strain in lead-free BNT-BT system modified with Al and Sb. *Materials Letters*. 2016;184:152-156.

15. Xiong Z, Tang B, Fang Z, Yang C, Zhang S. Effects of $(Cr_{0.5}Ta_{0.5})^{4+}$ on structure and microwave dielectric properties of $Ca_{0.61}Nd_{0.26}TiO_3$ ceramics. *Ceramics International*. 2018;44(7):7771-7779.

16. Lu X, Xu J, Yang L, Zhou C, Zhao YY, Yuan C, et al. Energy storage properties of $(Bi_{0.5}Na_{0.5})_{0.93}Ba0.0_7TiO_3$ lead-free ceramics modified by La and Zr co-doping. *Journal of Materiomics*. 2016;2(1):87-93.

17. Shi J, Yang W. Piezoelectric and dielectric properties of CeO_2-doped $(Bi_{0.5}Na_{0.5})_{0.94}Ba_{0.06}TiO_3$ lead-free ceramics. *Journal of Alloys and Compounds*. 2009;472(1-2):267-270.

18. Simons H, Daniels J, Jo W, Dittmer R, Studer A, Avdeev M, et al. Electric-field-induced strain mechanisms in lead-free 94%$(Bi_{1/2}Na_{1/2})TiO_3$-6%$BaTiO_3$. *Applied Physics Letters*. 2011;98(8):082901.

19. Nguyen VQ, Han HS, Kim KJ, Dang DD, Ahn KK, Lee JS. Strain enhancement in $Bi_{1/2}(Na_{0.82}K_{0.18})_{1/2}TiO_3$ lead-free electromechanical ceramics by co-doping with Li and Ta. *Journal of Alloys and Compounds*. 2012;511(1):237-241.

20. Zannen M, Lahmar A, Dietze M, Khemakhem H, Kabadou A, Es-Souni M. Structural, optical, and electrical properties of Nd-doped $Na_{0.5}Bi_{0.5}TiO_3$. *Materials Chemistry and Physics*. 2012;134(2-3):829-833.

21. Fu P, Xu Z, Chu R, Li W, Xie Q, Zhang Y, et al. Effect of Dy_2O_3 on the structure and electrical properties of $(Bi_{0.5}Na_{0.5})_{0.94}Ba_{0.06}TiO_3$ lead-free piezoelectric ceramics. *Journal of Alloys and Compounds*. 2010;508(2):546-553.

22. Li L, Xu M, Zhang Q, Chen P, Wang N, Xiong D, et al. Electrocaloric effect in La-doped BNT-6BT relaxor ferroelectric ceramics. *Ceramics International*. 2018;44(1):343-350.

23. Marwat MA, Xie B, Ashtar M, Zhu Y, Fan P, Zhang H. High remnant polarization, high dielectric constant and impedance performance of Nb/In Co-doped $Bi_{0.49}La_{0.01}Na_{0.49}Li_{0.01}TiO_3$-d ceramics. *Ceramics International*. 2018;44(6):6843-6850.

24. Zuo R, Ye C, Fang X, Li J. Tantalum doped $0.94Bi_{0.5}Na_{0.5}TiO_3$-$0.06BaTiO_3$ piezoelectric ceramics. *Journal of the European Ceramic Society*. 2008;28(4):871-877.

25. Xie B, Zhang Q, Zhang L, Zhu Y, Guo X, Fan P, et al. Ultrahigh discharged energy density in polymer nanocomposites by designing linear/ferroelectric bilayer heterostructure. *Nano Energy*. 2018;54:437-446.

26. Bai W, Li H, Xi J, Zhang J, Shen B, Zhai J. Effect of different templates and texture on structure evolution and strain behavior of <001>-textured lead-free piezoelectric BNT-based ceramics. *Journal of Alloys and Compounds*. 2016;656:13-23.

27. Liu X, Li F, Li P, Zhai J, Shen B, Liu B. Tuning the ferroelectric-relaxor transition temperature in NBT-based lead-free ceramics by Bi nonstoichiometry. *Journal of the European Ceramic Society*. 2017;37(15):4585-4595.

28. Li F, Chen G, Liu X, Zhai J, Shen B, Zeng H, et al. Phase-composition and temperature dependence of electrocaloric effect in lead-free $Bi_{0.5}Na_{0.5}TiO_3$-$BaTiO_3$-$(Sr_{0.7}Bi_{0.2}\square_{0.1})TiO_3$ ceramics. *Journal of the European Ceramic Society*. 2017;37(15):4732-4740.

29. Yu Z, Liu Y, Shen M, Qian H, Li F, Lyu Y. Enhanced energy storage properties of $BiAlO_3$ modified $Bi_{0.5}Na_{0.5}TiO_3$-$Bi_{0.5}K_{0.5}TiO_3$ lead-free antiferroelectric ceramics. Ceramics International. 2017;43(10):7653-7659.

30. Bai W, Chen D, Huang Y, Zheng P, Zhong J, Ding M, et al. Temperature-insensitive large strain response with a low hysteresis behavior in BNT-based ceramics. *Ceramics International*. 2016;42(6):7669-7680.

31. Liu X, Tan X. Giant Strains in Non-Textured $(Bi_{1/2}Na_{1/2})TiO_3$-Based Lead-Free Ceramics. *Advanced Materials*. 2016;28(3):574-578.

32. Fan P, Zhang Y, Xie B, Zhu Y, Ma W, Wang C, et al. Large electric-field-induced strain in B-site complex-ion $(Fe_{0.5}Nb_{0.5})^{4+}$-doped $Bi_{1/2}(Na_{0.82}K_{0.12})_{1/2}TiO_3$ lead-free piezoceramics. *Ceramics International*. 2018;44(3):3211-3217.

33. Bai W, Li L, Li W, Shen B, Zhai J, Chen H. Effect of $SrTiO_3$ template on electric properties of textured BNT-BKT ceramics prepared by templated grain growth process. *Journal of Alloys and Compounds*. 2014;603:149-157.

34. Pal V, Kumar A, Thakur OP, Dwivedi RK, Prasad NE. Preparation, microstructure and relaxor ferroelectric characteristics of BLNT-BCT lead-free piezoceramics. *Journal of Alloys and Compounds*. 2017;714:725-735.

35. Thawong P, Kornphom C, Prasertpalichat S, Pinitsoontorn S, Chootin S, Bongkarn T. Effect of firing temperatures on properties of BNT-BCTZ-0.007mol%BFCO lead free piezoelectric ceramics synthesized by the solid state combustion method. *Ceramics International*. 2017;43(Suppl 1):S172-S181.

36. Liao Y, Xiao D, Lin D, Zhu J, Yu P, Wu L, et al. Synthesis and properties of $Bi_{0.5}(Na_{1-x-y}K_xAg_y)_{0.5}TiO_3$ lead-free piezoelectric ceramics. *Ceramics International*. 2007;33(8):1445-1448.

37. Uchino K, Nomura S. Critical exponents of the dielectric constants in diffused-phase-transition crystals. *Ferroelectrics*. 1982;44(1):55-61.

38. Khemakhem L, Kabadou A, Maalej A, Ben Salah A, Simon A, Maglione M. New relaxor ceramic with composition $BaTi_{1-x}(Zn_{1/3}Nb_{2/3})_xO_3$. *Journal of Alloys and Compounds*. 2008;452(2):451-455.

39. Yang H, Yan F, Lin Y, Wang T, Wang F, Wang Y, et al. Lead-free $BaTiO_3$-$Bi_{0.5}Na_{0.5}TiO_3$-$Na_{0.73}Bi_{0.09}NbO_3$ relaxor ferroelectric ceramics for high energy storage. *Journal of the European Ceramic Society*. 2017;37(10):3303-3311.

40. Wang C, Lou X, Xia T, Tian S. The dielectric, strain and energy storage density of BNT-BKH_xT_{1-x} piezoelectric ceramics. *Ceramics International*. 2017;43(12):9253-9258.

41. Ullah A, Ahn CW, Malik RA, Kim IW. Dielectric and impedance spectroscopy of lead-free $0.99[(Bi_{0.5}Na_{0.4}K_{0.1})(Ti_{0.980}Nb_{0.020})O_3]$-$0.01(Ba_{0.7}Sr_{0.3})TiO_3$ ceramics. *Physica B: Condensed Matter*. 2014;444:27-33.

42. Li L, Hao J, Xu Z, Li W, Chu R, Li G. Large strain response in (Mn,Sb)-modified $(Bi_{0.5}Na_{0.5})_{0.935}Ba_{0.065}TiO_3$ lead-free piezoelectric ceramics. *Ceramics International*. 2016;42(13):14886-14893.